MEMS-Based Testing Stage to Study Electrical and Mechanical Properties of Nanocrystalline Metal Films

Jong H. Han, Jagannathan Rajagopalan, and M. Taher A. Saif
Dept. of Mechanical Science and Engineering, Univ. of Illinois at Urbana-Champaign, 1206 West Green Street, Urbana, IL USA 61801

ABSTRACT

We have developed a MEMS-based testing stage that can quantitatively characterize both the electrical and mechanical properties of nanocrystalline metal films. This stage, which is SEM and TEM compatible, is a modified version of an earlier MEMS-based tensile testing stage (M. A. Haque and M. T. A. Saif, *Proc. Natl. Acad. Sci*., 101(17), 6335-6340 (2004)). This modified stage requires a simpler fabrication procedure, involving less lithography and etching steps, and has higher sample yield compared to the earlier version. It allows for 4-point electrical resistivity measurement, and in-situ tensile testing in SEM and TEM of free-standing nano-scale metal films. The stage was used to perform a tensile test and electrical resistivity measurement on 100-nm-thick aluminum films, the results of which are described.

Keywords: In-situ uniaxial tensile, TEM, SEM, aluminum, electrical resistivity, nanocrystalline, MEMS

1. INTRODUCTION

The increased use of nanocrystalline metal films as interconnects in integrated circuits has necessitated their thermo-electro-mechanical characterization, as these films experience elevated temperatures and thermal stresses during device operation. It is well known that the deformation mechanisms in nanocrystalline metals deviates markedly from those in bulk metals.[1-3] Studying the mechanical and electrical response of nanocrystalline metal films under stress and increased temperature can provide fundamental insight into the physical processes active in these materials. However, performing experiments to investigate the deformation behavior of nanocrystalline metal films has always been a challenge due to the small size of the samples[4] and the limitations of the instrumentation.

To study the behavior of small scale materials, researchers have used various methods such as wafer curvature technique, nanoindentation, bulge testing, and uniaxial tensile-testing. Although these testing methods have been breakthroughs in testing miniaturized samples and widely utilized, they have limitations in simultaneously observing the qualitative and quantitative mechanical response of a material. The wafer curvature technique[5] employs the thermal mismatch between the film and the wafer substrate to induce deformation in the film. Therefore, the influence from the heating and the film/substrate interface can bring complexity into the data interpretation. Nanoindentation doesn't necessarily involve heating in testing, but the measurement may not be directly performed because of the specimen pile-up and sink-in, the substrate effect[6], and the roughness of the sample[7]. Also, testing beyond the elastic limit requires *a priori* model.

Bulge testing pressurizes one side of a free-standing membrane to use pressure-deflection relation to extract mechanical response, so no substrate effect is encountered.[8] However, the testing can be very sensitive to the slight misalignment between the loading and the sample.[9] Like the bulge testing, uniaxial tensile testing removes any substrate effects and allows studying the mechanical response with its stress and strain measured directly. In many cases, load cell is used to measure the stress, and some type of micro actuation is used to stretch a sample[10], and measuring the strain is done by using optical interference from photoresist islands on a sample[11], sample deflection[12], and metal markers.[13, 14] Although these types of techniques can provide quantitative measurement of stress and strain of a sample, the qualitative analysis of microstructural response in analytical chambers such as SEM, AFM, X-ray, and TEM is not easily allowed due to the large size of the test set-up.

MEMS/MOEMS Components and Their Applications IV, edited by Srinivas A. Tadigadapa, Reza Ghodssi, Albert K. Henning, Proc. of SPIE Vol. 6464, 64640C, (2007) · 0277-786X/07/$18 · doi: 10.1117/12.706115

Some uniaxial tensile experiments were carried out in the analytical chambers to study microstructural evolution during applying stress on the sample. An electrostatic force grip connected to a motor[15] and a needle hook with a piezoelectric actuator[16] was used to apply tension on a sample inside SEM. Uniaxial tensile testing was done under AFM for studying surface evolution during loading.[17] X-ray diffraction was also used in in-situ measurement of stress.[18-21] In-situ uniaxial tensile testing of nanocrystalline thin films with simultaneous measurement of stress-strain response and observation of microstructural changes in TEM became first possible with the MEMS-based micro tensile stage.[22-24] Some advantages of this stage include its compact size, accurate sample alignment, no-slip gripping, and displacement-based stress-strain measurement. However, the thin film samples that were cofabricated with the stage mostly failed during fabrication, and since the calibration of the force sensor of the stage involved a destructive method, the stage couldn't be reused.

To overcome these limitations with the in-situ tensile stage, a second generation stage has been developed and is introduced in this paper. The new design of the second generation stage enables 100% sample yield, and a new non-destructive technique of calibrating the force sensor is developed, which allows reuse of stage and calibration prior to testing. In addition, the second generation stage has built-in capability for 4-point electrical resistivity measurement of the nanocrystalline metal thin film. Therefore, with this stage, in-situ mechanical and electrical characterization in TEM and at different temperatures is possible. A new fabrication technique that requires fewer lithography and etching steps (half of that required for the first generation stage) is also presented. 100-nm-thick Al films with average grain size of 65 nm and 55 nm, respectively, are used to demonstrate the ability of the new stage to investigate deformation behavior and to measure electrical resistivity of thin nanocrystalline films.

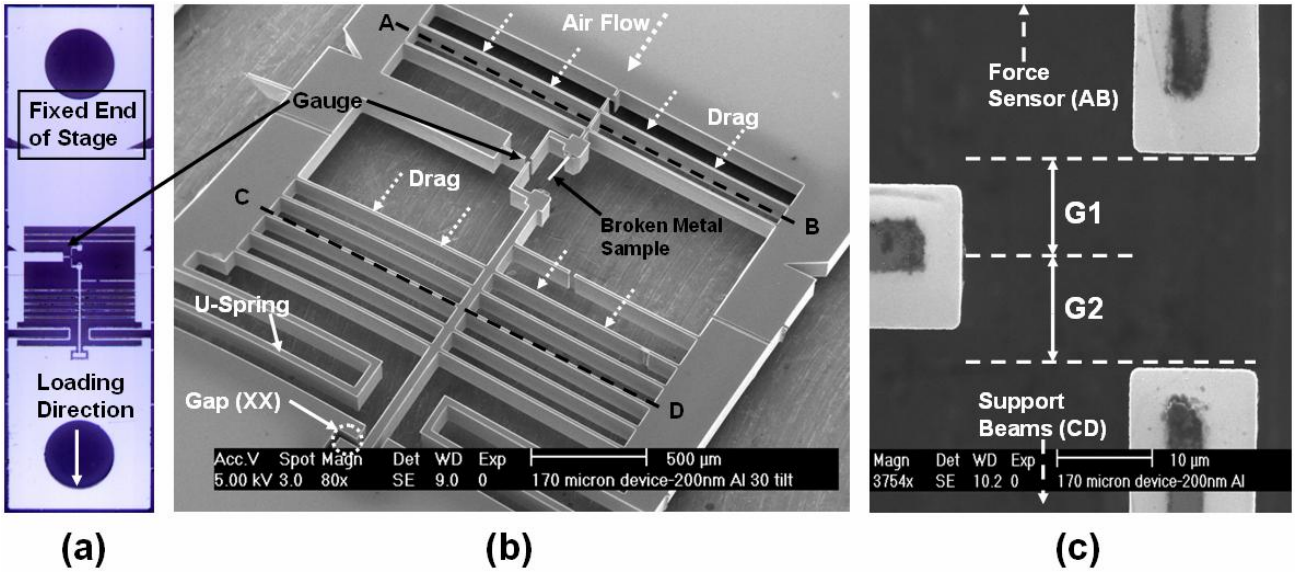

Fig. 1 First generation micro tensile stage: (a) optical microscope view of the stage; (b) SEM view of the stage showing major components. Air flow and drag effect on the beams are shown with dotted arrows.; (c) zoom-in view of the gauge.

2. DESIGN IMPROVEMENTS IN SECOND GENERATION STAGE

2.1 Description of MEMS-based Testing Stage

The first generation testing stage is described in Fig. 1. The stage is 10-mm long, 3-mm wide, and about 150-µm thick. The stage is composed of Si structures and a metal sample. The set of Si beams (AB) is the force sensor that deflects when force is applied to the specimen during testing. Multiplying the deflection by its stiffness gives the force and hence

the stress in the sample. The force sensor is calibrated by measuring its stiffness using nanoindentation. Another set of Si beams (CD) act as support beams that ensure proper alignment between the loading and sample axes. The U-beams allow for large extension of the stage while sustaining its mechanical integrity. The gap (XX) protects the sample against pre-testing damage coming from mishandling. When performing tensile tests in-situ in TEM, the gap is initially closed half way, which induces tension in the U-beams without deforming the sample. This tension in the U-beams holds the micro stage firmly onto the straining stage, precluding the need for extra clamping components. During tensile testing, the micro stage is stretched by anchors connected to external actuators such as a piezo or a motor. After the gap (XX) closes, any additional stretch will then be transferred to the sample, causing the sample to elongate and the force sensor to deflect. The sample elongation and the force are measured by the movement of the gauges. The change in the gap (G1) represents the deflection of the force sensor, and the elongation in the sample is obtained by subtracting the change in the gap (G1) from the change in the gap (G2). From these measurements, stress and strain of the sample can be directly calculated.

2.2 Design Changes for Sample Failure Reduction

It had been observed that most of the free-standing samples are fractured after the last part of the deep Si etching in an ICP DRIE chamber, during which the compliant Si beams as well as the free-standing samples are formed. During and after the etching process in ICP DRIE, the compliant structure and the sample are subjected to the drag force induced by the sudden air flow due to the pressure difference between the process chamber and loadlock upon gate opening for unloading. The drag on the Si beams of the tensile stage is described in Fig. 1 (b). The force sensor and the support beams are aligned perpendicular to the drag so that their movement under the influence of the drag force is the maximum compared to that of the other components of the tensile stage. The stiffness of the support beams is larger than that of the force sensor. Therefore, when the beams initially deflect due to the drag, the free-standing sample is compressed and hence buckles in the out-of plane direction because of its large length and small thickness. At this point, the sample does not break. However, after this initial deflection, the beams can deflect in the opposite direction as they undergo oscillation. During this reverse deflection, the sample is stretched, i.e., subjected to tensile deformation, and hence can fracture.

To prevent the sample from fracturing, a Si beam connecting the force sensing beams and the support beams was introduced in the second generation stage (Fig. 2(b)).[25] This rigid protecting beam ensures that the deflection of the support beams and the force beams are the same. Hence, the sample section behaves like as a rigid body, and hence no stresses are induced on the specimen. With the protecting beam added on to the tensile stage design, 100% sample yield rate was achieved. The protecting beam not only prevents the sample failure during fabrication but also minimizes any damages to the sample, which come from mishandling. The gauges that were separated by Si etching in the original design (Fig. 1 (c)) are kept connected throughout the etching process in the second generation stage as shown in Fig. 2 (c). The unetched gauges serve as the protecting beam, preventing the sample from failing.

In order to conduct tensile testing, the protecting beam needs to be disconnected so that the sample can elongate. This is accomplished by cutting the protecting beam with FIB. After FIB cutting, the protecting beam is used as gauges to measure stress-strain response (Fig. 2 (d)). Using FIB allows for forming small gauge gaps that are not achievable with conventional dry Si etching, in turn increasing the resolution of the measurements. Since the FIB cutting operation is performed in vacuum, it was necessary to examine whether the heat generated by the ion bombardment causes any damage such as recrystallization to the free standing metal sample. As microstructural change leads to changes in its electrical properties, the electrical resistance of the sample was measured before and after FIB cutting to check for any such changes. However, no noticeable change in resistance was observed. If there was any heating due to FIB cutting, the heat must have transferred to the Si body of the stage rather than to the sample, since the stage structure has a much larger mass and would behave as a heat sink.

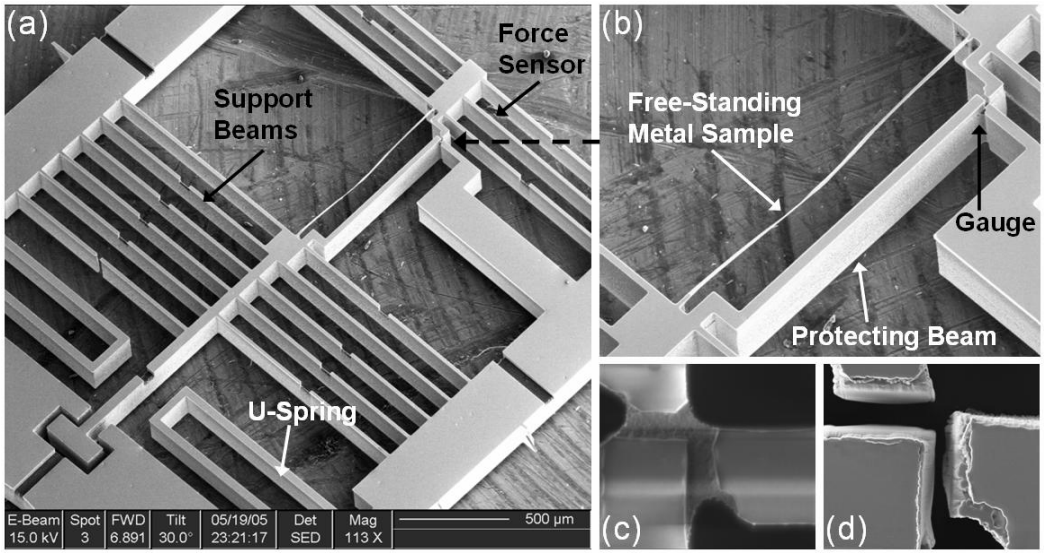

Fig. 2. Second generation micro tensile stage: (a) SEM view of the stage showing the major components; (b) zoom-in view near the free-standing sample and the gauge; (c) the gauge before and (d) after FIB cutting.

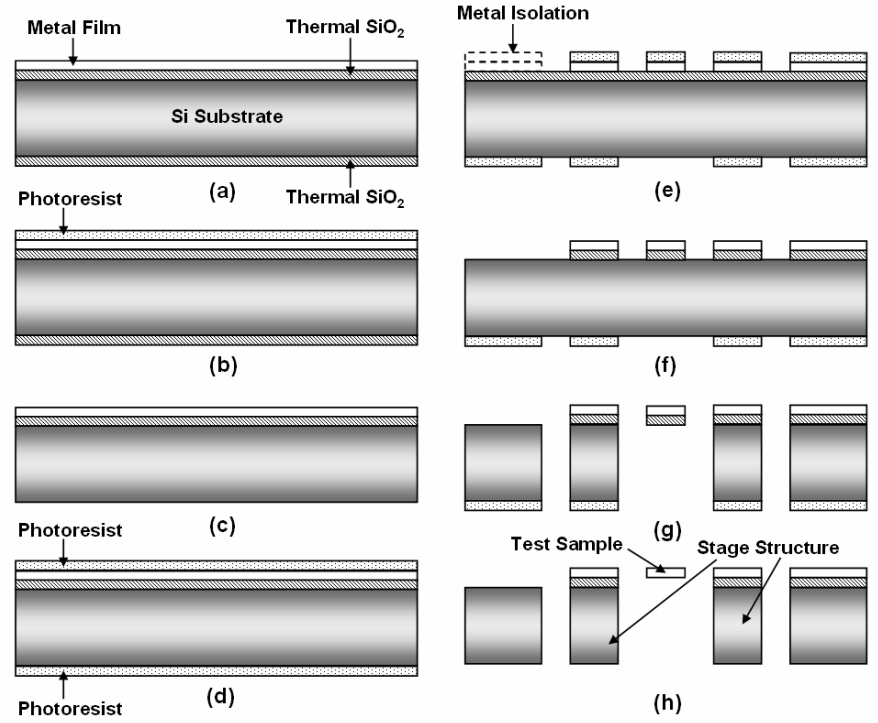

Fig. 3. Fabrication flow: (a) growing thermal SiO_2 layers on top and bottom of Si wafer and depositing metal film on top; (b) spincoating photoresist on top; (c) etching bottom SiO_2 in HF and removing photoresist on top; (d) spincoating photoresist on top and bottom; (e) patterning on top and bottom by photolithography and etching exposed metal layer in metal etchant. Top and bottom patterns are the mirror images except that the bottom pattern of the sample is open so that the sample becomes free-standing after deep Si etching done from the bottom. There are metal isolations in the top pattern, which are small regions with separation of metal and oxide in the direction perpendicular to the page to form paths for electrical current during 4-point resistivity measurement as showing in Fig. 5 (a).; (f) etching exposed SiO_2 and removing photoresist on top; (g) anisotropic deep Si etching from bottom; (h) removing SiO_2 underneath the sample and photoresist on bottom.[25]

3. FABRICATION AND FEATURES OF SECOND GENERATION STAGE

3.1 Fabrication Procedure

While the fabrication of the first generation tensile stage involved two metal deposition, three lithography, and three Si etching steps, a new fabrication technique that requires only one metal deposition, two lithography, and one Si etching step, was developed for the second generation MEMS tensile stage.[25] The schematic of the fabrication process is summarized in Fig. 3. The top metal coating serves as the tensile testing sample after being freed from the substrate. It is also used to act as electrodes and interconnects for 4-point resistivity measurement with patterned metal isolations on the top side of the wafer. The thermally grown SiO_2 layer acts as an electrical insulator to prevent the flow of current between the metal layer and the Si substrate. A coating of photoresist on top and bottom is used to pattern the micro tensile stage with optical lithography. The bottom photoresist layer also serves as a mask for deep Si etching in ICP DRIE. The thickness of the Si wafer is the thickness of the tensile stage. At the location of the sample, the bottom pattern has an opening, allowing the deep Si etching to release the sample from the Si substrate and become free-standing.

3.2 New Calibration Technique

Calibration of the force sensor for the first generation stage required cleaving of the stage in order to expose the force sensor to a nanoindenter. Therefore, the calibration can only be done after testing, and both the stage and the sample are destroyed. Also, cleaving involves the risk of damaging the force sensor. The calibration technique for the second generation stage has been changed, allowing the sample and the stage to be reused and the calibration to be done prior to testing.[25] Figure 4 shows the sequence of the calibration steps. Two Si-based calibrators connected to mounting dies (Fig. 4 (a)) are fabricated in a same batch with the tensile stages. One of them, calibrator (i), is cut from the mounting die and glued onto a platform, and the stiffness of the leaf spring is measured by nanoindentation. Then, the calibrator (i) is used to calibrate the leaf spring of the calibrator (ii) (Fig. 4 (b)). After that, the calibrator (ii) is cut from its mounting die and placed inside the tensile stage as showing in Fig 4 (c). The calibrator is pushed against the force sensor, with the deflection of its leaf spring and the force sensor being measured by the calibrator gauge and the stage gauge, respectively. With the stiffness of one of the deflecting Si beams known, stiffness of the other beam can be calculated by the technique shown in Fig. 4(d). The guide and the aligner on the stage and the calibrator minimize rotation of the calibrator when the calibrator moves.

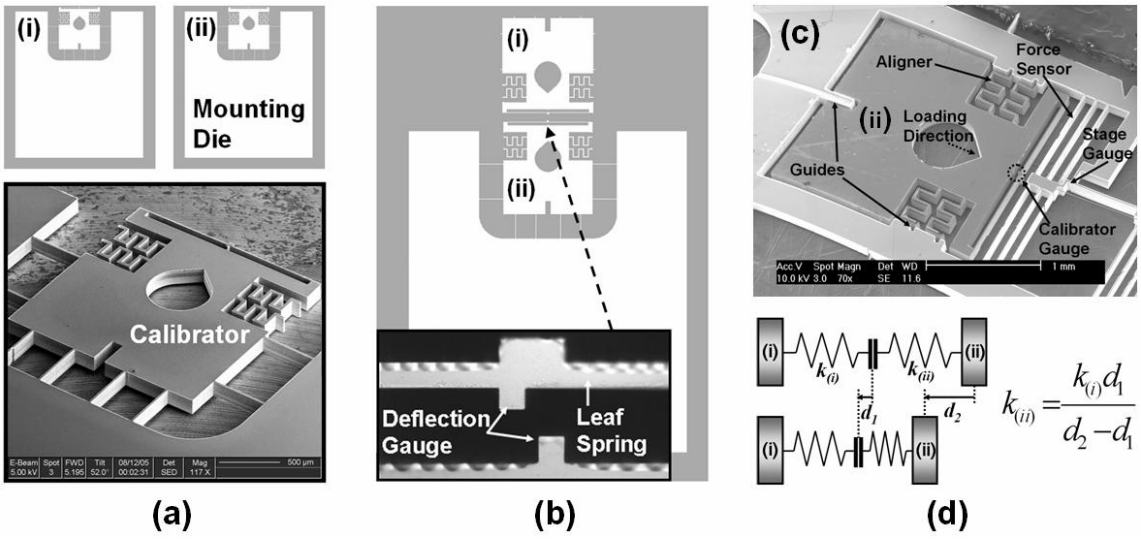

Fig. 4.Calibration procedure: (a) CAD view of the calibrator with the mounting die. Bottom picture is a SEM shot of the calibrator; (b) calibration of the calibrator (ii) using the calibrator (i) after nanoindentation (Inset is a close-up view at the gauge.); (c) calibration of the force sensor using the calibrator (ii); (d) schematic representation of the calibration technique.[25]

3.3 Built-in Function for 4-point Resistivity Measurement

The second generation stage has built-in capability for 4-point resistivity measurement.[25] Figure 5 shows the pathways for the applied current and the voltage measurement, as well as the schematic describing the principle of the 4-point resistivity measurement technique. These pathways are formed by electrical isolations on the metal film on top. Using this technique excludes the effect of contact resistance at the electrodes, R_1-R_4. The ratio of the measured voltage to the current supplied gives the resistance of the free-standing metal sample, R_S. SiO_2 layer between the metal coating and the Si substrate prevents the current from flowing across the thickness of the stage.

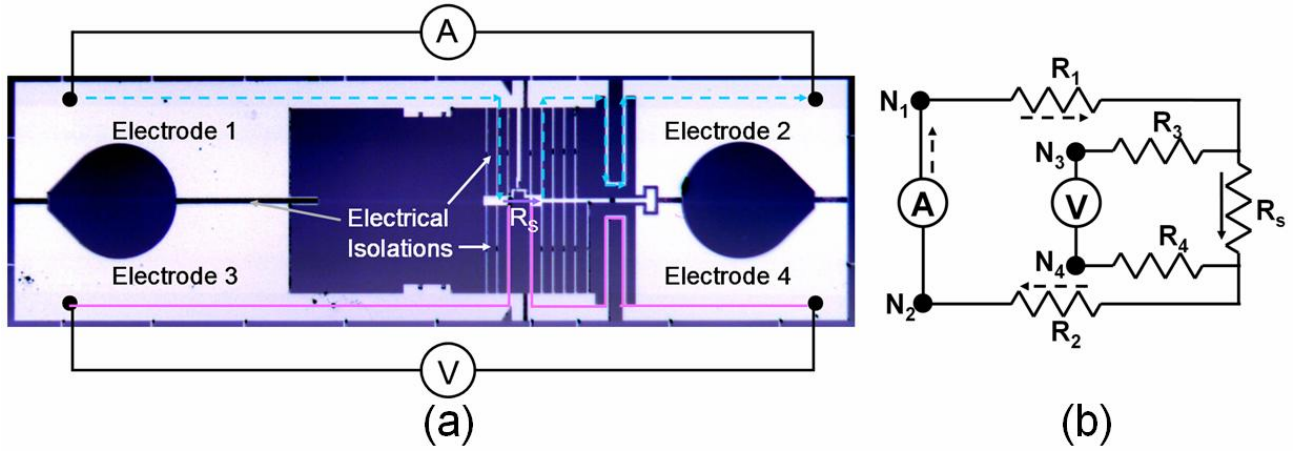

Fig. 5. 4-point resistivity measurement using the micro tensile stage; (a) Schematic of the current flow and voltage measurement on the stage; (b) Electrical circuit formed on the stage, with arrows indicating the direction of the electrical current flow. [25]

4. RESULTS AND DISCUSSIONS

Two Al samples were prepared for mechanical and electrical characterization. Both of the Al samples were sputter-deposited at 7.1nm/min rate with 300-W power, and the base pressure of the chamber was about 10^{-7} Torr. For the uniaxial tensile testing, an Al film of 100-nm thickness and with average grain size of 65 nm was deposited on a bare Si wafer. For the 4-point resistivity measurement, an Al film of 100-nm thickness and with average grain size of 55 nm was deposited on a thermally grown SiO_2 layer. The tensile testing sample was 810-nm-long and 13-μm-wide. The spring constant of the force sensor using the calibration method discussed in the previous section was measured to be 64 N/m, and the elastic modulus was 61 GPa.[25] The stress-strain response is shown in Fig. 6 (a).

Figure 6 (b) shows the result of the 4-point resistivity measurement of the Al sample at different temperatures. Each data point was attained after allowing hot plate temperature to stabilize for each increase of temperature. Then, the voltage was measured upon applying 2 μA of current for 20 seconds, and the sample resistance was calculated from the ratio of the voltage measured over the current supplied. After reaching 116 ^{o}C, the sample was cooled down to room temperature. The resistivity prior to annealing is about 0.23 μohm-m, which is nine times larger than that of bulk Al (0.0262 μohm-m). The resistivity increases with heating and decreases with cooling. Upon cooling, resistivity value reaches its original value before annealing. 4-point resistance measurement on the micro stage with a broken Al sample gave resistance values four orders of magnitude larger than that with the sample alive, which implies that the resistivity value measured in Fig. 6 (b) is solely that of the free-standing Al sample.

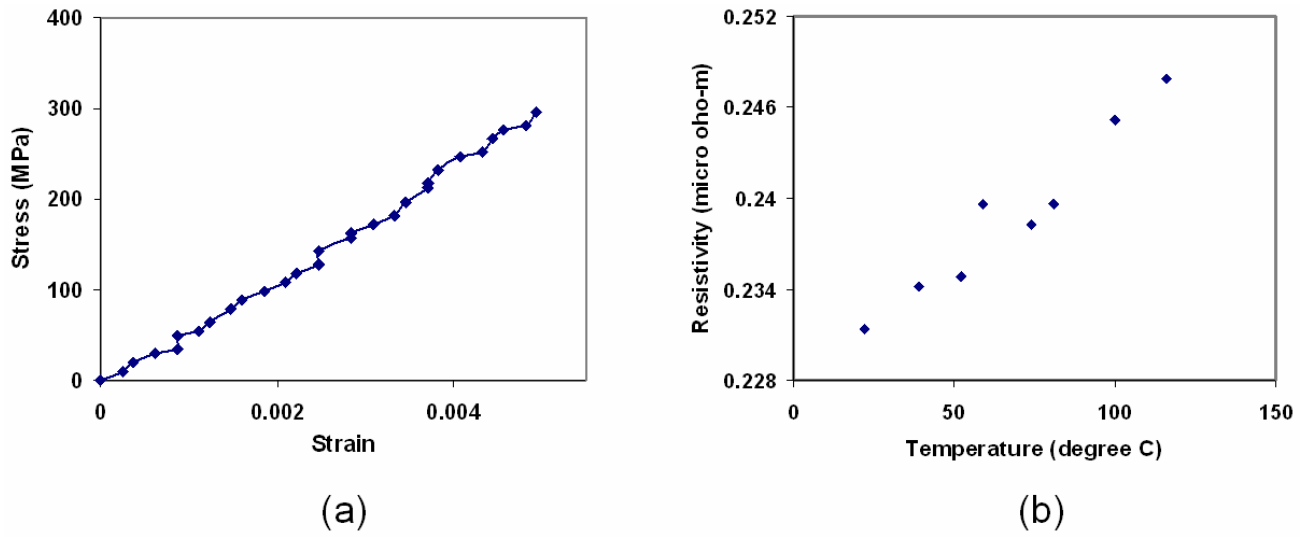

Fig. 6. Experimental results: (a) stress- strain curve for 100-nm-thick Al sample [25]; (b) resistivity of 100-nm-thick Al sample as a function of temperature.

5. CONCLUSIONS

This paper presents the second generation of the MEMS-based testing stage originally introduced in [24]. The testing stage allows in-situ quantitative study and microstructural observation during uniaxial tensile testing of nanocrystalline free-standing metal thin films in SEM and TEM. The new design implemented in the 2nd generation stage enables 100% yield of metal samples while allowing the force sensor to be calibrated before testing without breaking the stage or the sample. Also, the fabrication process has been improved, by reducing the number of metal deposition, lithography, and Si etching steps. Furthermore, 4-point resistivity measurement capability has been built into the second generation stage. Therefore, with proper electrical connections equipped on a TEM stage, one can conduct a uniaxial tensile testing while measuring the resistivity of the sample and observing microstructural evolution under stress in-situ in TEM. Uniaxial tensile test and 4-point resistivity measurement at varying temperatures were performed on nano-grained Al samples using the second generation testing stage. The elastic modulus was found to be 61 GPa, and an increase in the resistivity was observed with temperature. The initial resistivity was about nine times higher than the bulk value.

ACKNOWLEDGMENTS

The research involved for this paper was funded by NSF grant ECS 97-34368, DMR 0237400, and AFOSR grant USAF-5212-STI-SC-0004. Fabrication of micro tensile stages was carried out in Micro-Nano Technology Laboratory and Micro-Miniature Systems Lab of University of Illinois at Urbana-Champaign. Valuable discussions with Khalid Hattar and Prof. Ian Robertson in the Department of Materials Science & Engineering of UIUC are appreciated.

REFERENCES

1. C. A. Neugebauer, "Tensile properties of thin, evaporated gold films," *J. Appl. Phys*., 31, 1096-1101 (1960).

2. M. Y. Gutkin, I. A. Ovid'ko, and C. S. Pande, "Theoretical models of plastic deformation processes in nanocrystalline materials," *Rev. Adv. Mater. Sci.*, 2, 80-102 (2001).

3. E. Artz, "Size effects in materials due to microstructural and dimensional constraints: a comparative review," *Acta Mater*., 46(16), 5611-5626 (1998).

4. M. J. Madou, "Fundamentals of microfabrication," CRC Press (1997).

5. P. A. Flinn, D. S. Gardner, and W. D. Nix, "Measurement and interpretation of stress in aluminum-based metallization as a function of thermal history," *IEEE Trans. Electron Devices*, 3, 689-699 (1987).

6. W. D. Nix, "Mechanical properties of thin films," *Metall. Trans*., 20A, 2217-2245 (1989).

7. T. Ting,, PhD Thesis, Mechanical Engineering and Materials Science, Rice University, 1997.

8. Y. Xiang, X. Chen, and J. J. Vlassak, "The plane-strain bulge test for thin films," *J. Mater. Res*., 20(9), 2360-2370 (2005).

9. R. W., Hoffman, "Nanomechanics of thin films: emphasis: tensile properties," *MRS Symp. Proc*., 130, 295-305 (1989).

10. D. Y. W. Yu and F. Spaepen, "The yield strength of thin copper films on Kapton," J. Appl. Phys., 95(6), 2991-2997 (2004).

11. J. A. Ruud, D. Josell, and F. Spaepen, "A new method for tensile testing of thin films," *J. Mater. Res*., 8(1),112-117 (1993).

12. H. D. Espinosa, B. C. Prorok, and M. Fischer, "A methodology for determining mechanical properties of freestanding thin films and MEMS materials," *J. Mech. Phys. Solids*, 51, 47–67 (2003).

13. B. Yuan and W. N. Sharpe, "Mechanical testing of polysilicon thin films with the ISDG," *Expt. Tech*., 21(2), 32-35 (1997).

14. K. M. Jackson, J. Dunning, C. A. Zorman, and W. N. Sharpe, "Mechanical properties of epitaxial 3C silicon carbide thin films," *J. Microelectromech. Syst*., 14(4), 664-672 (2005).

15. T. Tsuchiya, O. Tabata, J. Sakata, and Y. Taga, "Surface-micromachined polycrystalline silicon thin films," *J. Microelectromech. Syst*., 7(1), 106-113 (1998).

16. D. T. Read, Y. Cheng, R. R. Keller, and J. D. McColskey, "Tensile properties of free-standing aluminum thin films," *Scr. Mater*., 45,583-589 (2001).

17. I. Chasiotis and W. G. Knauss, "A new microtensile tester for the study of MEMS materials with the aid of atomic force microscopy," *Expt. Mech*., 42(1), 51-57 (2002).

18. P.O. Renault, P. Villain, C. Coupeau, Ph. Goudeau, and K. F. Badawi, "Damage mode tensile testing of thin gold films on polyimide substrates by X-ray diffraction and atomic force microscopy," *Thin Solid Films*, 424(2), 267-273 (2003).

19. K. F. Badawi, P. Villain, Ph. Goudeau, and P.-0. Renault, "Measuring thin film and multilayer elastic constants by coupling in-situ tensile testing with x-ray diffraction," *Appl. Phys. Lett*., 80(25), 4705-4707 (2002).

20. O. Kraft, M. Hommel, and E. Arzt, "X-ray diffraction as a tool to study the mechanical behaviour of thin films," *Mater. Sci. Eng. A*, 288(2), 209-216 (2000).

21. J. Bohm, P. Gruber, R. Spolenak, A. Stierle, A. Wanner, and E. Arzt, "Tensile testing of ultrathin polycrystalline films: a synchrotron-based technique," *Rev. Sci. Inst*., 75(4), 1110-1119 (2004).

22. M. A. Haque and M. T. A. Saif, "Application of MEMS force sensors for in-situ mechanical characterization of nano-scale thin films in SEM and TEM," *Sensors and Actuators A*, 97-98, 239-245 (2002).

23. M. A. Haque and M. T. A. Saif, "Mechanical behavior of 30-50 nm thick aluminum films under uniaxial tension," *Scr. Mater*., 47(12), 863-867 (2002).

24. M. A. Haque and M. T. A. Saif, "Deformation mechanisms in free-standing nanoscale thin films: a quantitative in-situ transmission electron microscope study," *Proc. Natl. Acad. Sci*., 101(17), 6335-6340 (2004).

25. J. H. Han and M. T. A. Saif, "In situ microtensile stage for electromechanical characterization of nanoscale freestanding films," *Rev. Sci. Inst.,* 77(4), 45102-1-8 (2006).